Korean J. Chem. Eng., 39(5), 1257-1267 (2022)
DOI: 10.1007/s11814-021-1031-x

pISSN: 0256-1115
eISSN: 1975-7220

Simultaneous removal of Congo red and Cr(VI) using amino-modified GO/MS composite materials

Liang Cheng*,†, Li Zhang, Hongxia Wang**, and Fangxiang Song****

*School of Electrical Engineering, Guizhou University, Guiyang 550025, China
**College of Chemistry and Chemical Engineering, Guizhou University, Guiyang 550025, China
(*Received 3 August 2021 • Revised 31 October 2021 • Accepted 29 November 2021*)

Abstract−Mesoporous silica (MS) and graphene oxide (GO) are good absorbents. Combining them not only prevents GO agglomeration but increases the number of MS active sites. In addition, their composites can preferentially adsorb specific pollutants after modification. In this work, amino-modified GO/MS materials were prepared by post-grafting to remove Congo red (CR) and Cr(VI) in solution. Characterization methods, such as X-ray diffraction (XRD), transmission electron microscopy (TEM), Fourier transform infrared spectroscopy (FTIR), Zeta potential, and N_2 adsorption/desorption, were adopted. The prepared GO/MS@HBP has a porous structure with a specific surface area of 49.32 $m^2 \cdot g^{-1}$. The effect of initial concentration, pH, adsorption time, temperature and other ions was determined on the adsorption amount. Relying on this, the GO/MS@HBP maximum capacity for Cr(VI) and CR adsorption are 93.73±2.3% and 257.69+1.5% $mg \cdot g^{-1}$, respectively. Pseudo-second-order kinetic and Langmuir isotherms are more suitable to describe the adsorption process, indicating that chemical adsorption plays a major role in the entire adsorption process. Thermodynamics showed that the enthalpy (H) of materials adsorbing two pollutants was positive and that the Gibbs free energy (G) was negative, suggesting that Cr(VI) and CR adsorption on GO/MS@HBP was spontaneously endothermic. GO/MS@HBP could simultaneously remove CR and Cr(VI) in solution, and be an effective adsorbent for removing harmful substances.

Keywords: Postgrafting Method, Mesoporous Silica, Graphene Oxide, Adsorption, Cr(VI), Congo Red

INTRODUCTION

Water is an important resource for survival. However, with the development of modernization and industrialization, it is necessary to address water pollution. Wastewater containing dyes and heavy metal ions is worth noting. Dye wastewater has high chroma, a complex composition, and poor reproducibility. These characteristics further damage plants, animals and even humans [1-3]. Congo red is a type of dye, and its degradation byproducts have carcinogenic effects. It is harmful to human skin, eyes, blood and germ cells. It may affect blood coagulation and cause drowsiness and respiratory problems [4,5]. On the other hand, hexavalent chromium is a heavy metal ion that causes nonnegligible damage to plants [6], humans [7], organisms and soil [8,9]. Congo red (CR) and Cr(VI) have mutagenesis, carcinogenesis, and teratogenesis effect on the human body. CR is a typical representative of azo dyes, which affects the quality of water bodies and the health of aquatic organisms. In addition, chromium, a widely used industrial heavy metal, is one of the three internationally recognized carcinogenic metals and a priority control pollutant. These two pollutants have serious effects on the ecological environment balance and health. Therefore, based on the above reasons, CR and Cr(VI) were selected as the research objects.

To remediate the pollution caused by Congo red and hexavalent chromium, many methods have emerged. Recently, the common methods of Congo red removal have been chemical [10], adsorption [11], and physical methods [12]. Common methods for removing Cr(VI) include the chemical precipitation [13], ion exchange [14], electrochemical treatment [15] and adsorption [16]. Among these methods, adsorption is not only fast, economical, and easy, but also has universality and could be used for soluble, insoluble and biological pollutants [17]. The choice of adsorbent is important in treating pollutants. Common adsorbents include activated carbon, silica gel, macroporous resins and so on, but they still have unsatisfactory adsorption effects. For example, they are expensive and difficult to renew and easily cause problems, such as secondary pollution [18]. Secondly, some composite materials are also used as adsorption materials to remove Congo Red and Cr(VI) at the same time. Zhang et al. [19] prepared Fe_3O_4@Carbon composites to simultaneously remove Congo red and Cr(VI), and the maximum adsorption capacity of Cr(VI) and Congo red was 33.35 mg g^{-1} and 262.72 mg g^{-1}, but this composite material needs to be obtained at high temperature, this process increases cost and energy consumption. Mohammad et al. [20] prepared cellulose acetate/chitosan/SWCNT/Fe_3O_4/TiO_2 composite nanofibers to remove Cr(VI), As(V), Methylene blue and Congo red and obtained good adsorption effect; however, the material system and process were complicated. Bakry et al. [21] prepared bentonite/chitosan@cobalt oxide composite to remove of Congo red dye and Cr(VI) from water, and the maximum adsorption capacity was 303 mg g^{-1} and 250 mg g^{-1}, respectively. Although the composite material had a good adsorption effect, it was easy to cause secondary pollution.

†To whom correspondence should be addressed.
E-mail: 1972600120@qq.com

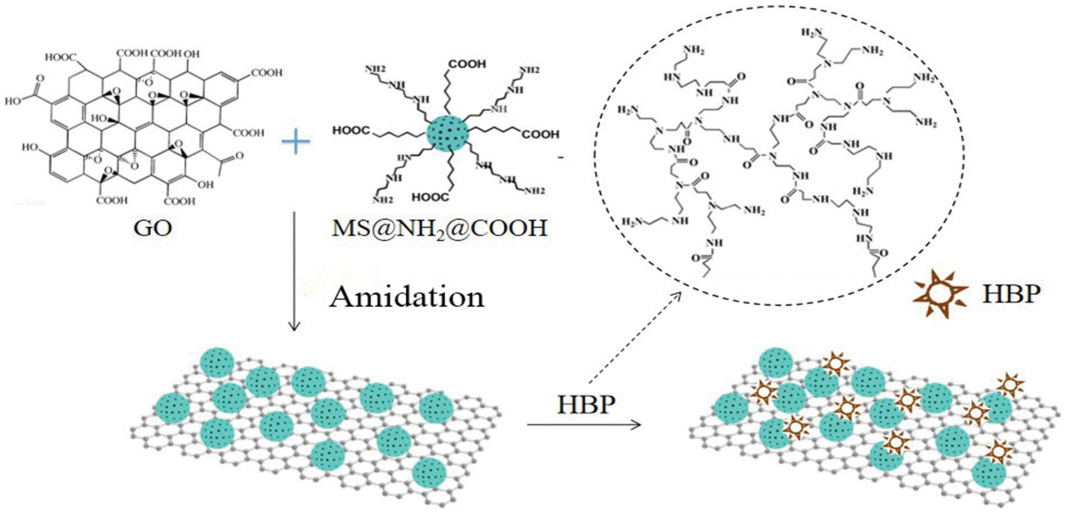

Scheme 1. Preparation of GO/MS@HBP by the postgrafting method.

Thus, a low-cost, low energy consumption, and high-efficiency adsorbent material needs to be developed.

As one such adsorbent, graphene oxide has a high oxygen content in its graphite-derived layer (graphene oxide). In addition, carbonyl and carboxyl groups are located on the edge of graphene oxide sheets. Graphene oxide also contains hydroxyl and epoxyl groups on its surface [22], and the existence of these groups makes it hydrophilic and easy to disperse in water [23]. Due to the large surface area of graphene oxide, it is useful for removing heavy metal ions and dyes [24]. However, graphene oxide also has disadvantages. Even with high-speed centrifugation, graphene oxide remains difficult to completely recycle from a well-dispersed solution, which limits its practical application in wastewater treatment [25]. Mesoporous silica nanoparticles (MSNs) are composed of porous channels. They are important nanomaterials that have attracted interest in materials science. By combining graphene oxide and mesoporous silica [26], the shortcomings of graphene are solved, and mesoporous silica could also provide active sites. Li et al. prepared mesoporous silica-grafted graphene oxide nanomaterials to selectively adsorb Pb(II) from 14 metal ions, and the removal rate was greater than 99% [27]. Modifying GO/SiO_2 materials could enhance their adsorption capacity. Amino groups are the most widely used and most effective modification group, and amino-modified materials also exhibit good Cr(VI) and CR adsorption [28,29]. Stimulus responsive hyperbranched polymers (HBP) with terminal amino groups have large amino groups and branches.

In this work, spherical mesoporous silica (MS) was successfully functionalized with polyamines and cyanogen. Then, an amidation reaction was carried out between GO and modified MS, and the product was named GO/MS@NH_2@CN. After cyanogen was functionalized on MS hydrolyzed to carboxyl groups, HBP was grafted onto MS through an amidation reaction. The final product, GO/MS@HBP, was used to adsorb Cr(VI) and CR. Then, the influencing factors (pH, reaction time, adsorbent dose, initial concentration and competitive adsorption), adsorption model, adsorption dynamics and thermodynamics were explored. Ultimately, we used FT-IR, TG-DSC, XRD, BET, SEM, and zeta potential, etc. to characterize GO/MS@HBP. The preparation of GO/MS@HBP by the postgrafting method is shown in Scheme 1.

EXPERIMENTAL

1. Materials

Cetyl trimethylammonium bromide (CTAB), absolute ethyl alcohol, methylbenzene, and Congo red were purchased from Tianjin KGM Chemical Reagent Co., Ltd. (China). Tetraethoxysilane (TEOS) and ammonium hydroxide were purchased from Chengdu Jinsan Chemical Reagent Co., Ltd. (China). Sulfuric acid was purchased from Chongqing Chuandong Chemical Co., Ltd. (China). 1-(3-Dimethylaminopropyl)-3-ethylcarbodiimide hydrochloride (EDC), 1,3,5-trimethyl benzene (TMB), graphite powder, and N-hydroxy succinimide (NHS) were purchased from Aladdin Industrial Corporation (Shanghai, China). 2-Morpholinoethanesulfonic acid monohydrate (MES) was purchased from Beijing Solaibao Technology Co. Ltd. (China). 3-(2-(2-aminoethylamino)ethylamino)propyl-trimethoxysilane (NQ-62) was purchased from Shanghai Macklin Biochemical Co., Ltd. (China). 2-Cyanoethyltriethoxysilane (CTES) was purchased from TCI (Shanghai, China). Tris(hydroxymethyl) aminomethane (Tris) and potassium dichromate were purchased from Tianjin Fuyu Fine Chemical Co. Ltd. (China). Bromohexadecyl pyridine (CPB) was purchased from Shanghai Macklin Biochemical Co., Ltd. (China). Deionized water (DW) used in all experiments was made in the laboratory. All chemical reagents were of analytical grade and purchased without further purification.

2. Preparation of GO/MS@HBP by Postgrafting

MS@NH_2@COOH was prepared by a method similar to that described in our previous work [30]. Preparation and functionalization of mesoporous silica (MS) spheres: MES (0.9 g) was added to 6 mL of acetone, and a mixture of DW (58 mL) and ethanol (16 mL) was added. Next, 0.2 g of NaCl was added and stirred until it was dissolved completely. Ammonia (275 μL), CTAB (0.4505 g) and tris (0.25 g) were added at 35 °C, then, 0.1 g of CPB and 1 mL of TMB were added with vigorous stirring for 30 min. Afterwards, 2.355 mL of TEOS was gradually added for another 24 h. Then,

30 mL of acetone was added at 50 °C for 1 h. After repeated washing with DW and ethanol and vacuum drying, we obtained mesoporous silica (MS) spheres.

Preparation of MS@NH_2@CN: One gram of MS was ultrasonically dispersed in 50 mL of anhydrous toluene, and then, 1.3 mL of NQ-62 was added and refluxed at 100 °C for 11 h. Furthermore, 1.8 mL of CTES was added and stirred for 24 h to obtain MS@NH_2@CN.

Preparation of GO/MS@HBP: 40 mg of GO was ultrasonically dispersed in 100 mL of DW. To obtain GO/MS@NH_2@CN, 60 mg of EDC, 40 mg of NHS and 250 mg of MS@NH_2@CN were added at 35 °C for 24 h. Then, after ultrasonicating for 10 min, a dilute sulfuric acid solution (1 : 1) was added to the mixture. The product was named GO/MS@NH_2@COOH. After dispersing GO/MS@NH_2@COOH in ethanol, an ethanol solution (20 mg·L^{-1}) dissolved in HBP was quickly added, and then, the mixture was reacted at 74 °C overnight. The final product GO/MS@HBP was obtained after suction filtration, washing and vacuum drying.

3. Material Characterization

Scanning electron microscopy (SEM, SIGMA+X-MaxN, Germany) was used to observe the morphology of the materials by determining the material surface properties with microscopic imaging. The pretreatment of the sample was to first disperse it in anhydrous ethanol and dry it in a vacuum, place the dried sample on the conductive glue, and spray gold in a vacuum evaporator. Transmission electron microscopy (TEM, FEIG20) is a characterization method to observe the inner structure of samples. The pretreatment of the sample was fully ultrasonically dispersed in anhydrous ethanol, using a dropper to suck up the evenly mixed solution, dropping it on the microgrid, repeat 2-3 times, and fully drying the sample. X-ray diffraction (XRD, X'Pert Powder, the Netherlands) was used to study the crystal structure of the materials and analyze the phase of the materials by analyzing the diffraction patterns of the materials. The test conditions of the sample were Cu$K\alpha$ rays as the radiation source, the scanning speed, scanning range, the tube pressure and tube flow were 2.4 s/step, 3-90°, 40 kV and 20 mA, respectively. Functional groups can be identified by analyzing Fourier transform infrared spectroscopy (FT-IR, VERTEX 70) spectra. Before the test, we took a very small amount of sample and mixed it with a certain amount of fully dried potassium bromide (about 1 : 100), then pressed the tablet after fully grinding. The wave number range was 40-4,000 cm^{-1}. Nitrogen adsorption-desorption isotherms were measured at −196 °C using a Micromeritics ASAP2010 (USA) to analyze the porous materials. The pretreatment conditions were vacuum degassing at 120 °C for 12 h. ζ-Potential (Delsa NanoZ) measurements were used to determine the charge distribution on the surface of the materials. The sample was dispersed ultrasonically in deionized water before testing, and adjusted to the required pH value with dilute hydrochloric acid or dilute sodium hydroxide. Thermogravimetric-differential scanning calorimetry (TG-DSC) (STA 449C Jupiter, Germany) was used to characterize the prepared materials. Under the protection of nitrogen, the measurement temperature was increased at a rate of 10 °C/min, and the measurement temperature range was 30-1,000 °C.

4. Adsorption Experiment

GO/MS@HBP was used to adsorb CR and Cr(VI). For the adsorption of Cr(VI), 20 mg of GO/MS@HBP was added to 20 mL of a solution containing different concentrations of Cr(VI) at room temperature. Then, 5 mg, 10 mg, 20 mg, 30 mg, 40 mg, and 50 mg GO/MS@HBP were added to the 20 mL solution (100 mg·L^{-1} CR). After adsorption and centrifugation, the absorbances (CR and Cr(VI)) were measured at wavelengths of 496 nm and 540 nm using a UV spectrophotometer. Then, we explored the effects of initial concentration, pH, adsorption time, and different temperatures on the adsorption capacity and removal rate. In addition, we explored whether MB, XO, Cu(II), Ni(II), and Zn(II) in the solution influenced CR and Cr(VI) adsorption.

The removal rate and adsorption capacity of Cr(VI) and CR could be calculated according to the following formula [31]:

$$R = \frac{C_0 - C_t}{C_0} \times 100 \quad (1)$$

$$Q_t = \frac{(C_0 - C_t)V}{M} \quad (2)$$

where R is the removal rate of Cr(VI) and CR; C_0 and C_t are the initial and equilibrium concentrations of Cr(VI) and CR in the solution (mg·L^{-1}); Q_t is the adsorption capacity when adsorption reaches equilibrium (mg·g^{-1}); V is the volume of the adsorbed solution (L); and M is the mass of adsorbent used for adsorption (mg).

5. Regeneration Performance Research Experiment

GO/MS@HBP that adsorbed CR and Cr(VI) was added into HCl (0.05 mol·L^{-1}), which was used as the desorbent and shaken for 24 h (150 rpm) at room temperature. After repeated washing, vacuum drying was performed. Then, we obtained the recyclable adsorbent material. After three cycles, the concentration of CR and Cr(VI) after adsorption was finally measured with an ultraviolet spectrophotometer.

RESULTS AND DISCUSSION

1. Structure Characterization

The morphologies of GO/MS and GO/MS@HBP are displayed in Fig. 1(a), (b), which clearly depicts that GO/MS prepared by the post-grafting method is spherical mesoporous silica distributed on the GO flakes. There is no change in morphology after grafting HBP. Fig. 1(c) shows that GO is a lamellar structure with folded edges. Fig. 1(d) shows that the mesoporous silica spheres contain a worm-like pore structure, and the silica spheres are attached to the graphene oxide sheet, which also directly indicates that the structure never changed after modification.

The XRD pattern of the material is shown in Fig. 2. The characteristic peak of GO appears at 2θ=10.88°, showing that the interlayer spacing is 0.82 nm, which is slightly higher than the interlayer spacing of single-layer graphene. This may be because GO contains functional groups such as hydroxyl and carboxyl groups, indicating that the prepared GO was almost completely oxidized. GO/MS was modified by cyano, carboxyl or HBP, which have similar steamed bread peaks at 2θ=22°. The result was attributed to the amorphous SiO_2. Due to the amorphous SiO_2 adhering to the GO flakes, which inhibits the aggregation of GO flakes, leading to GO's

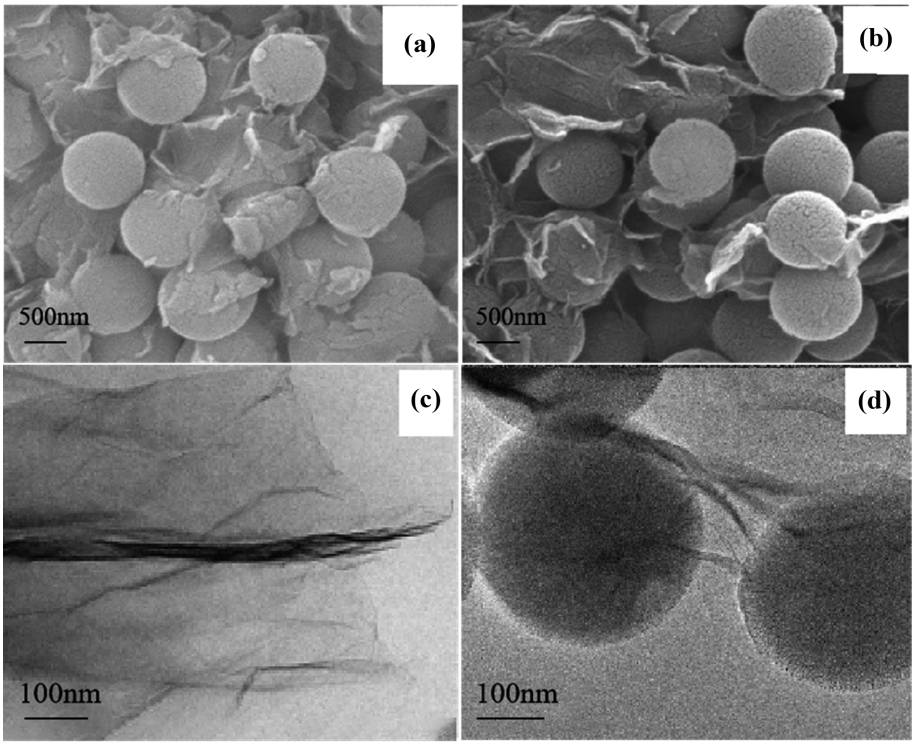

Fig. 1. SEM images of GO/MS (a) and GO/MS@HBP (b), TEM images of the prepared GO (c) and GO/MS@HBP (d) materials.

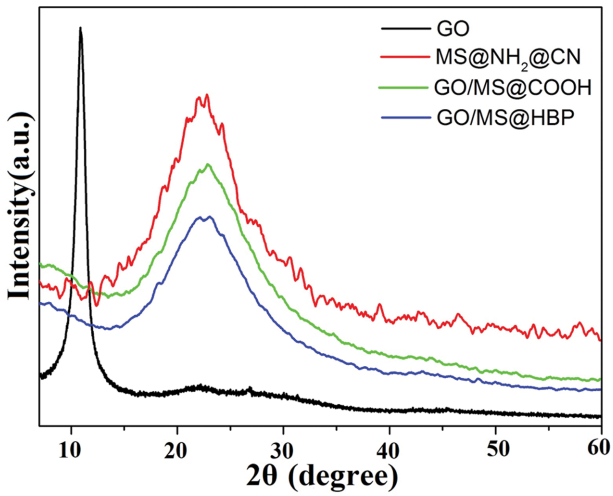

Fig. 2. The X-ray diffraction pattern of the material.

(001) crystal plane diffraction peak disappearing.

As shown in Fig. 3(b), the GO/MS, GO/MS@COOH and GO/MS@HBP isotherms exhibit characteristics of type I and type IV isotherms. The type I at low pressure indicates the existence of micropores, and the type IV with H4 type hysteresis loop suggests the existence of mesopores containing slit pores. From the pore size distribution diagram Fig. 3(a) and Table S1, the specific surface area, pore size and pore volume of the materials are reduced after modification; this is because the presence of the side chain organic chain covalently bonded to the inorganic network can partially prevent the entry of nitrogen molecules [32], indicating that the modified groups were successfully grafted. In addition, the pore sizes of GO/MS, GO/MS@COOH and GO/MS@HBP are distributed between micropores and mesopores.

The FT-IR spectra of the materials are shown in Fig. 4. The Si-O peak is located at 466 cm^{-1} from GO/MS, and the peak at 1,090 cm^{-1} is the asymmetric stretching vibration peak of Si-O-Si [33], expressing the existence of mesoporous silica. The peak at 2,258 cm^{-1} corresponds to the -CN in GO/MS@CN [34]. However, the -CN peak has no appearance in the FT-IR spectrum of GO/MS@COOH. The peak attributed to the carboxyl group appeared at 1,725 cm^{-1}, proving that the cyano group was successfully hydrolyzed to the carboxyl group. In the spectrum of GO/MS@HBP, the peak at 1,570 cm^{-1} is attributed to the NH bending vibration of the $-NH_2$ on the HBP [35]. The amino group reacting with the carboxyl group on GO/MS@COOH might explain the amide I band at 1,632 cm^{-1} [34], proving that the HBP was successfully grafted onto GO/MS@COOH. In our previous research [36], the change of FTIR spectrum after removal Congo Red and Cr(VI) was explained in detail.

The change of mass before and after modification could be obtained by thermogravimetric analysis. According to Fig. 5, the weight losses of the physically adsorbed water and chemically bound water of GO/MS@CN and GO/MS@HBP are 12.65% (Fig. 5(a)) and 9.89% (Fig. 5(b)), respectively, at range of 30-120 °C. GO/MS@CN has a weight loss of approximately 16.72% (Fig. 5(a)) at 120-500 °C, which corresponds to the weight loss of the cyano group and the alkyl chain. The subsequent weight loss is attributed to the condensation of silanol groups on the surface. The 15.34% weight loss of GO/MS@HBP at 120-400 °C is attributable to the weight loss of the amino groups on the HBP and the alkyl chain,

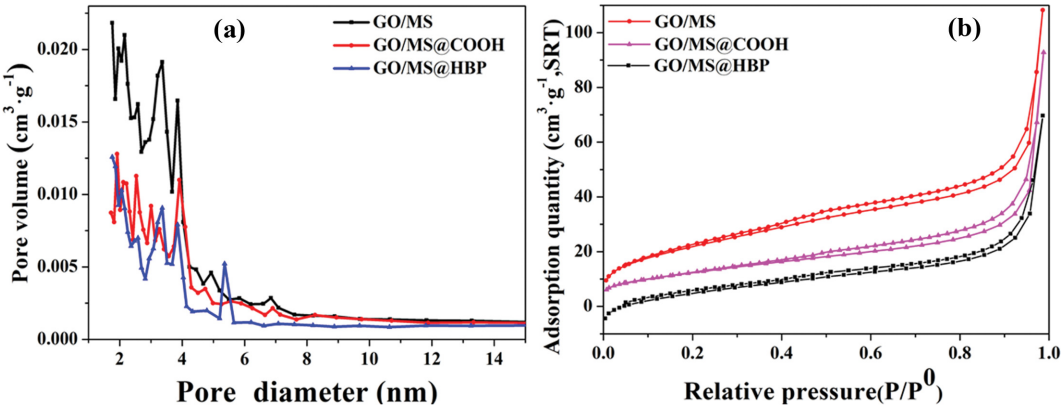

Fig. 3. Nitrogen adsorption isotherm (a) and pore size distribution (b) of the materials.

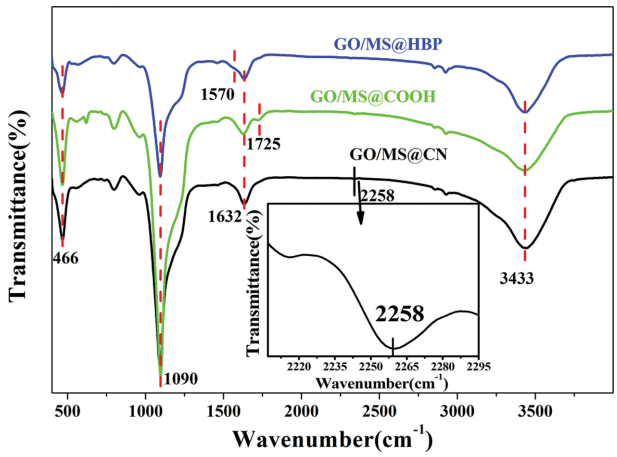

Fig. 4. FT-IR spectra of GO/MS@CN, GO/MS@COOH and GO/MS@HBP.

which was consistent with the maximum decomposition rate of the DTG curve at approximately 370 °C (Fig. 5(b)).

As shown in Fig. 6(a), the modified mesoporous silica spheres with amino groups and cyano groups are positively charged with 11.07 mV. When the MS@NH_2@CN have an amidation reaction with GO, they are negatively charged of −3.16 mV due to the existence of negative groups on graphene oxide. GO/MS@HBP is positively charged with 2.84 mV, indicating that the HBP was successfully grafted. In Fig. 6(b), the pHpzc of GO/MS@HBP is 7.78. At pH< 7.78, the material is positively charged. At pH>7.78, the material exhibits a negative charge.

2. Adsorption Research

2-1. Effect of the Different pH

The molecular form of CR changed with changing the solution pH value. At pH 2-4, CR is dark blue. At pH 10-12, CR is not the same as that in the original solution. Therefore, the experiment explored the adsorption performance of GO/MS@HBP in a CR solution with pH equal to 5, 6, 7, 8, and 9. Fig. 6(b) shows that the pHpzc of GO/MS@HBP is 7.78. At pH 5-7.78, the positive charge GO/MS@HBP attracted anionic CR. At pH 7.78-9, GO/MS@HBP was negatively charged, leading to GO/MS@HBP and CR being mutually exclusive. However, the adsorption capacity and removal rate had not obviously decreased (Fig. 7(a)). This may be due to the formation of hydrogen bonds between -NH_2 in GO/MS@HBP and the O, N, S, and benzene rings of the CR molecule. Thus, pH does not have much influence on the removal rate and adsorption capacity. Cr(VI) ions exist the forms of $H_2Cr_2O_7$, $Cr_2O_7^{2-}$, $HCrO_4^-$, CrO_4^{2-}, and $HCr_2O_7^-$ [37]. When the pH was less than 2, the main form was $H_2Cr_2O_7$; at pH 2-6, $Cr_2O_7^{2-}$ and $HCrO_4^-$ were the primary forms. When the pH was more than 7, CrO_4^{2-} was domi-

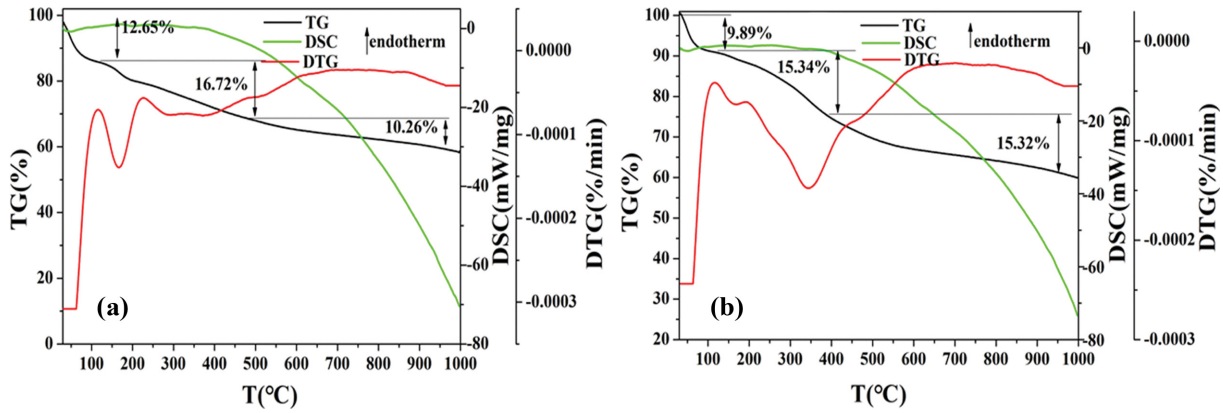

Fig. 5. Thermogravimetric curves of GO/MS@CN (a) and GO/MS@HBP (b).

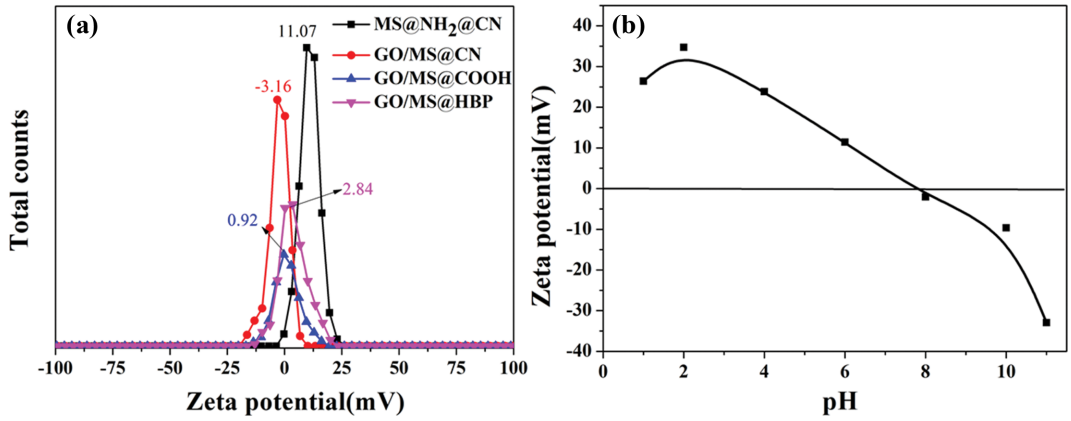

Fig. 6. The Zeta potential of the material (a) and the zeta potential of GO/MS@HBP under different pH conditions (b).

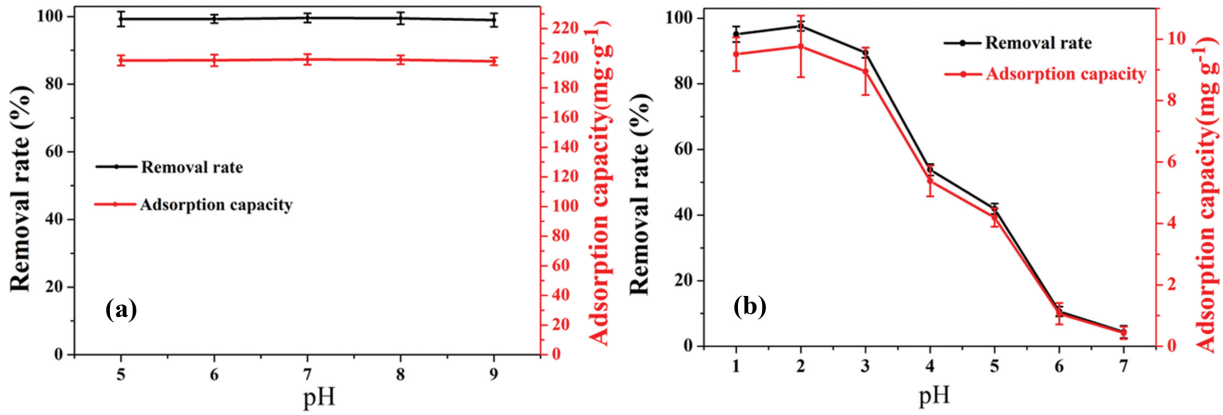

Fig. 7. Effect of the different pH values of GO/MS@HBP on CR (a) and Cr(VI) (b) adsorption.

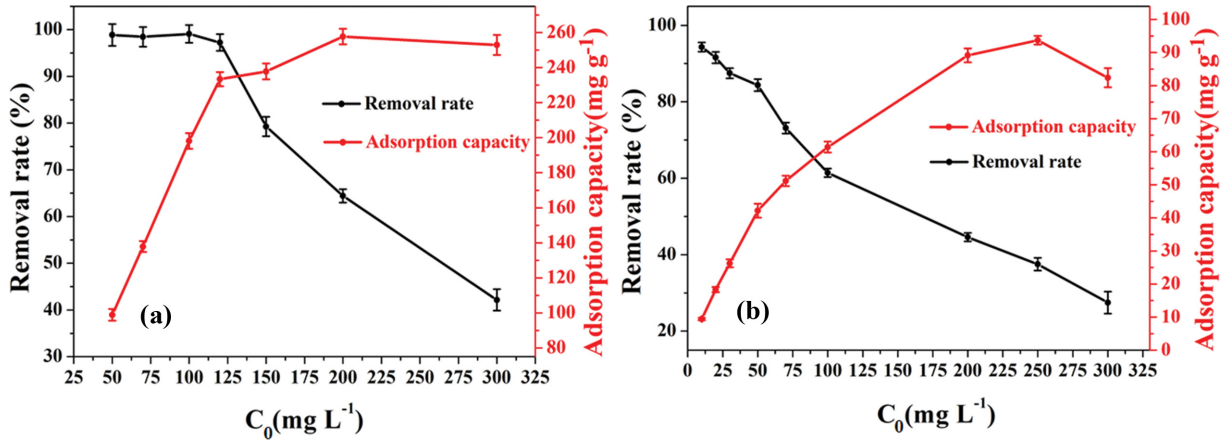

Fig. 8. Effect of the initial concentration of GO/MS@HBP on CR (a) and Cr(VI) (b) adsorption.

nant. Fig. 7(b) illustrates that with increasing pH, the adsorption capacity and removal rate of Cr(VI) by GO/MS@HBP decreased. At pH 2, the adsorption capacity and removal rate reached maximums. Fig. 6(b) shows that the pHpzc of GO/MS@HBP is 7.78. When the pH 2-7.78, the amino groups on the surface are positively charged because of protonation. However, as the pH increases, the zeta potential of GO/MS@HBP decreases gradually. Under this condition, Cr(VI) exists in the form of $Cr_2O_7^{2-}$ and $HCrO_4^-$. Although electrostatic attraction existed, the protonation degree of the amino groups and the active sites both reduced; thus, the adsorption capacity was decreased.

2-2. Effect of the Initial Concentration

As shown Fig. 8(a), as the initial concentration of CR increased the adsorption capacity decreased slightly, while the removal grad-

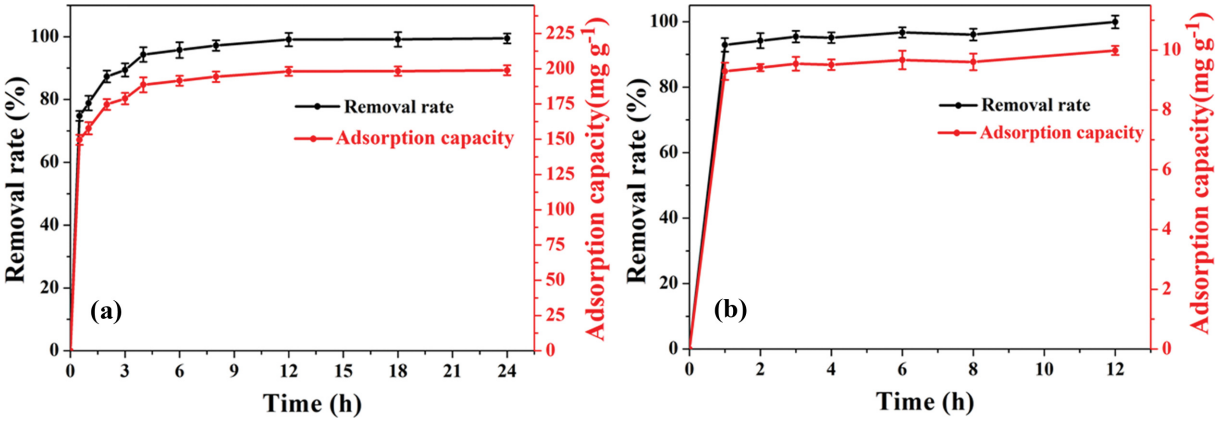

Fig. 9. Effect of the adsorption time of GO/MS@HBP on CR (a) and Cr(VI) (b) adsorption.

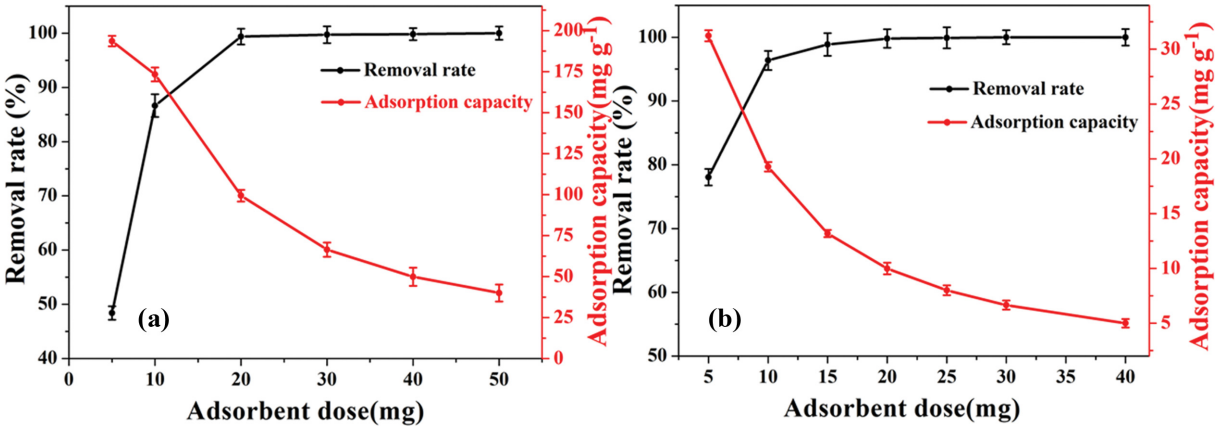

Fig. 10. Effect of the GO/MS@HBP absorbent dose on CR (a) and Cr(VI) (b) adsorption.

ually decreased. With the same amount of adsorbent, there were fewer CR molecules in the solution, amino groups formed hydrogen bonds with CR molecules. As the concentration increased, the amino groups that could be used for adsorption were inadequate and could not provide enough active sites for the CR molecules, so the removal rate decreased. As shown Fig. 8(b), with the increase in the initial concentration of Cr(VI), the adsorption capacity decreased slightly, and the removal rate gradually decreased. For the same amount of adsorbent, there were enough amino groups present at a lower Cr(VI) concentration. As the concentration increased, the amino groups were lacking. The adsorbent could not provide enough active sites for Cr(VI); therefore, the removal rate decreased.

2-3. Effect of the Adsorption Time

Fig. 9(a) shows that as time increases, the removal rate of CR and the adsorption capacity of CR gradually increases. This is due to the number of active sites rapidly increased initially. Adsorption reached saturation after 8 h. The saturated adsorption capacity and removal rate were 198.93±1.67% $mg \cdot g^{-1}$ and 99.46%, respectively. Similarly, because there was an adequate number of active sites, GO/MS@HBP removed over 90% of Cr(VI) within 1 h (Fig. 9(b)), the adsorption capacity reached 9.88±2.4% $mg \cdot g^{-1}$. The growth rate slowed as saturation was reached at 12 h, and the final removal rate was almost 100%. The adsorption capacity reached 10±2.1% $mg \cdot g^{-1}$.

2-4. Effect of Absorbent Amount

Fig. 10(a) shows that the CR and Cr(VI) removal rate of GO/MS@HBP gradually increases with increasing the adsorbent dose among 5-20 mg and the CR and Cr(VI) removal rate remains constant among 20-50 mg adsorbent dose, while the adsorption capacity gradually decreases. Insufficient numbers of active sites may be the reason why the adsorption rate at higher adsorbent doses was higher and larger than that at lower adsorbent doses. Therefore, it was necessary to select an appropriate amount of adsorbent to achieve higher adsorption capacity and removal rate. When the adsorbent dose is 50 mg, the removal rate is close to 100%. Considering the removal rate and adsorption capacity results, 10 mg of GO/MS@HBP was the best dose for adsorbing CR. Fig. 10(b) shows that the Cr(VI) removal rate of GO/MS@HBP gradually increases with increasing the adsorbent dose among 5-25 mg and the Cr(VI) removal rate remains constant among 25-40 mg adsorbent dose, while the adsorption capacity gradually decreases. When the adsorbent dose was small, the number of active sites for Cr(VI) was insufficient, resulting in incomplete adsorption and a low adsorption rate. When the adsorbent dose was excess, Cr(VI) was adsorbed completely. However, there were other sites on the surface of the adsorbent, so adsorption could not reach satura-

tion, which resulted in a low adsorption amount. As shown in Fig. 10(b), 5 mg of GO/MS@HBP could only achieve a removal rate of more than 77%. Overall, 20 mg of GO/MS@HBP was suitable in the experiment. The excellent adsorption performance of this material is better than that of other materials (Table S2).

3. Competitive Adsorption

Rhodamine B (RB), methylene blue (MB) and xylenol orange (XO) were used to compete with CR during adsorption. 10 mg of GO/MS@HBP was added to the mixed solution and shaken at room temperature for 12 h. Finally, the removal rates measured before and after are shown in Fig. S1. The CR peak after adsorption is dramatically reduced or has even disappeared, while the MB and XO peaks still exist, indicating that CR has been almost totally removed (Fig. S1(a), (b), (c), (d)). This is good proof that GO/MS@HBP has a good selectivity for CR. The Cu(II), Ni(II), and Zn(II) as heavy metal ions were used to compete with Cr(VI) for adsorption. The adsorption results of Cr(VI) in different mixtures are shown in Fig. S1(e). The presence of Cu(II), and Zn(II) had little influence on the removal rate of Cr(VI). In addition, the removal rate reached more than 94% for Cr(VI).

4. Adsorption Kinetics Study

The pseudo-first-order and pseudo-second-order kinetics models of GO/MS@HBP for the adsorption of CR and Cr(VI) help us understand the adsorption behavior. The pseudo-first-order and the pseudo-second-order kinetics models were applied to analyze the physicochemical processes in adsorption. The specific equations of the two models are as follows [38]:

$$\ln(q_e - q_t) = \ln q_e - K_1 t \quad (3)$$

$$\frac{t}{q_t} = \frac{1}{K_2 q_e^2} + \frac{t}{q_t} \quad (4)$$

where q_e and q_t (mg·g^{-1}) are the equilibrium adsorption capacity and adsorption capacity at time t, respectively, and K_1 and K_2 are the pseudo-first-order and the pseudo-second-order kinetic constant, respectively.

The fitting curves and related parameters are shown in Fig. 11 and Table 1. The fitting curves of the adsorption of CR and Cr(VI)

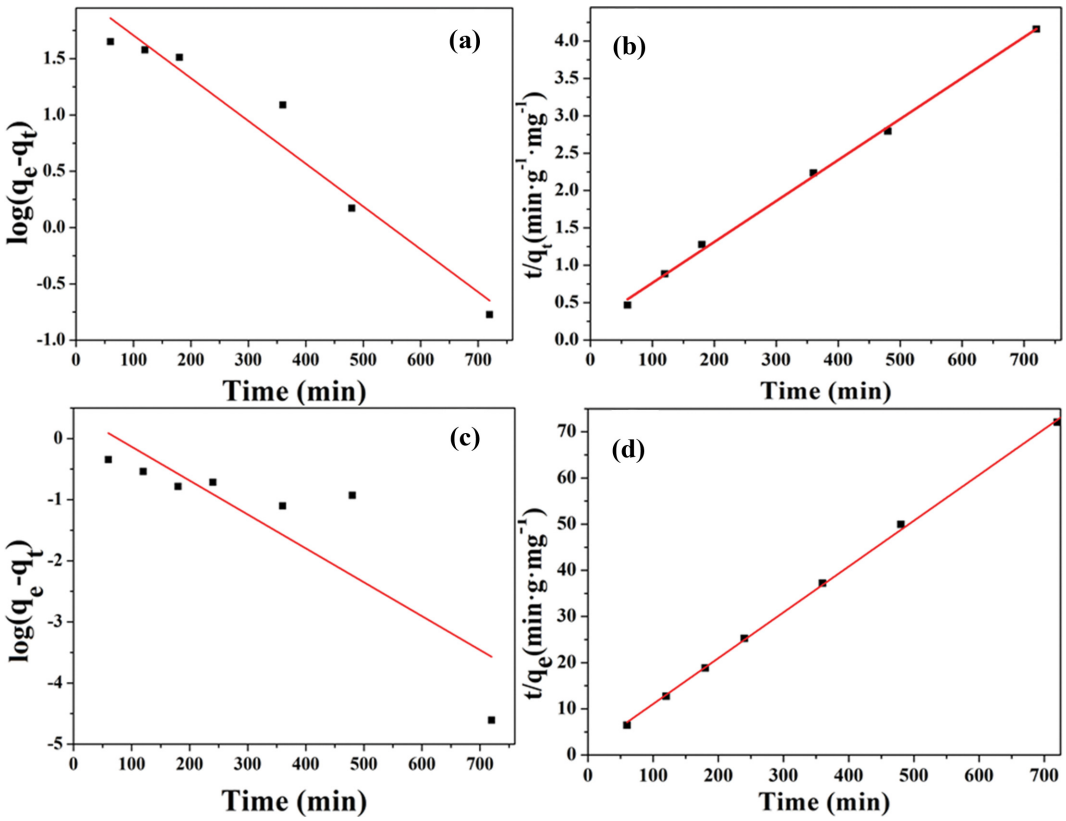

Fig. 11. Pseudo-first-order models and pseudo-second-order models of CR (a), (b) and Cr(VI) (c), (d) adsorption on GO/MS@HBP.

Table 1. The kinetic parameters of CR and Cr(VI) adsorption on GO/MS@HBP prepared by the postgrafting method

Adsorbates	C_0 (mg L^{-1})	q_e (mg g^{-1})	Pseudo-first-order kinetics			Pseudo-second-order kinetics		
			K_1 (min^{-1})	$Q_{e,cal}$ (mg g^{-1})	R^2	K_2 (min^{-1})	$Q_{e,cal}$ (mg g^{-1})	R^2
CR	100	198.93±1.67%	0.00444	41.23±2.5%	0.9265	0.0003	201.21±1.82%	0.99994
Cr(VI)	10	10±2.1%	0.01276	2.64±1.5%	0.6939	0.00864	10.08±2.15%	0.99984

are more coincident with the pseudo-second-order kinetic model, and the fitting coefficient of the pseudo-second-order kinetic model is more than 0.999, indicating that this process is mainly chemical adsorption and contains physical adsorption, which benefits from the large specific surface area of the material. The adsorption mechanism of Cr(VI) on GO/MS@HBP might be explained as: Through the electrostatic interaction between the negatively charged forms of Cr and the -NH_2 of GO/MS@HBP; in addition, Cr(VI) was reduced to Cr(III) and provided electron in the amino group, then Cr(III) was chelated on the amine groups [39,40]. For CR, it can interact with GO/MS@HBP by electrostatic attraction, and CR is an anionic ion dye with SO^{3-} groups and the benzene rings, making it to interact with GO. Besides, it is easy to form hydrogen bonds between -NH_2 in GO/MS@HBP and the O, N, S, and benzene rings of the CR molecule.

5. Adsorption Isotherms Study

The adsorption isotherm is frequently employed to evaluate the adsorption characteristics of an absorbent and analyze adsorption process. We used the Langmuir and Freundlich adsorption isotherms to understand the adsorption behavior of GO/MS@HBP to CR and Cr(VI). The equations of the Langmuir and Freundlich model are given as follows [41,42]:

$$\frac{C_e}{q_e}=\frac{C_e}{q_m}+\frac{1}{K_L q_m} \tag{5}$$

$$\ln q_e=\ln K_F+\frac{1}{n}C_e \tag{6}$$

$$R_L=\frac{1}{1+bC_0} \tag{7}$$

where q_e is the equilibrium adsorption capacity ($mg\cdot g^{-1}$); C_e is the solution concentration when adsorption reaches equilibrium ($mg\cdot L^{-1}$); q_m is the maximum adsorption capacity ($mg\cdot g^{-1}$); K_L is the Langmuir adsorbing equilibrium constant; b is the Langmuir constant in $L\cdot mg^{-1}$, and C_0 is the initial solution concentration; Among them, K_F and 1/n are Freundlich model parameters that represent adsorption capacity and adsorption intensity.

As shown in Fig. 12 and Table 2, the Langmuir model has a

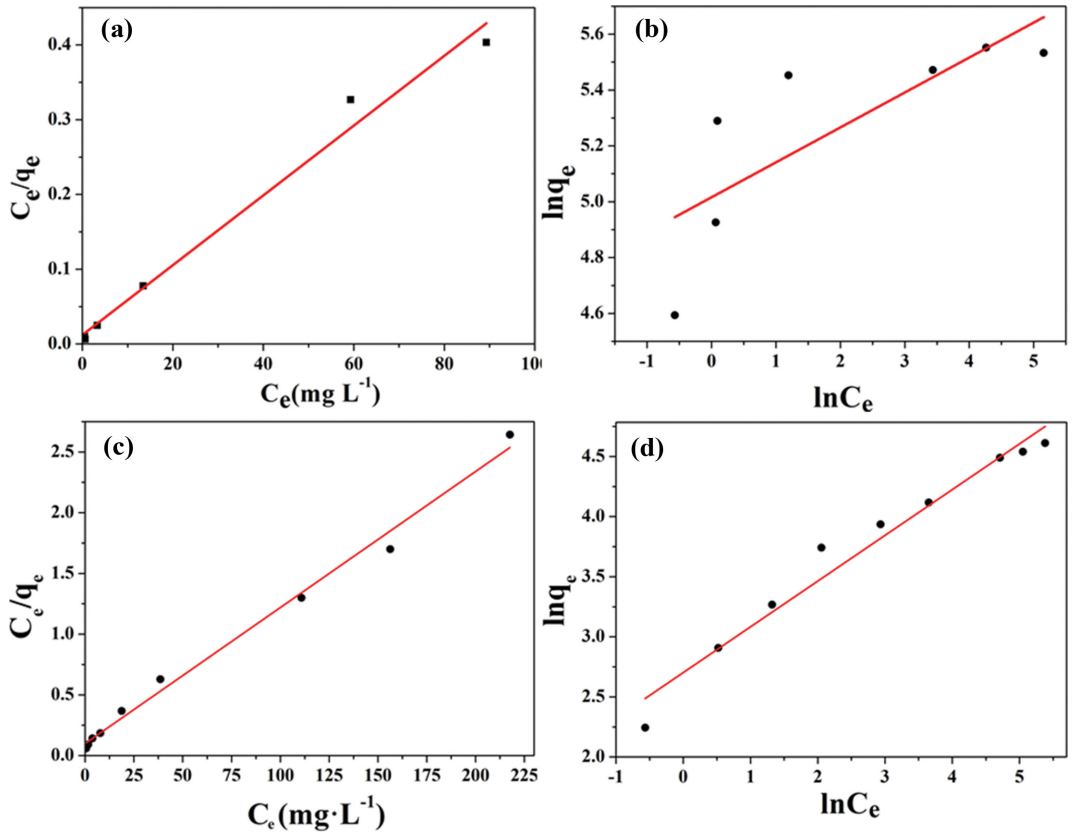

Fig. 12. Langmuir and Freundlich isotherms for CR(a) and (b), Cr(VI) (c) and (d) adsorption on GO/MS@HBP.

Table 2. The adsorption isotherm parameters of the Langmuir and Freundlich models of CR and Cr(VI) adsorption on GO/MS@HBP

Adsorbates	T (K)	Langmuir adsorption isotherm equation				Freundlich adsorption isotherm equation		
		q_m (mg g^{-1})	K_L (L mg^{-1})	R^2	R_L	1/n	K_F (L mg^{-1})	R^2
CR	298	257.69±1.5%	1.4943	0.999	0.002226-0.02607	0.1250	150.81	0.548
Cr(VI)	298	93.73±2.3%	0.1133	0.991	0.02858-0.4688	0.3805	14.91	0.963

Table 3. The thermodynamic parameters of CR and Cr(VI) adsorption on GO/MS@HBP prepared by the postgrafting method

Adsorbates	T (K)	ΔG^0 (kJ mol^{-1})	ΔH^0 (kJ mol^{-1})	ΔS^0 (kJ mol^{-1})
CR	298	−13.4018	26.2322	0.133
	308	−14.7318		
	318	−16.0618		
Cr(VI)	298	−62.3245	6.0069	0.2293
	308	−64.6175		
	318	−66.9105		

higher fitting coefficient than the Freundlich model. Hence, the Langmuir model is more suitable to describe adsorption behavior of the CR and Cr(VI) on GO/MS@HBP, suggesting that the adsorption type is single-layer adsorption. The obtained R_L value was between 0 and 1, indicating that GO/MS@HBP was beneficial to the adsorption of CR and Cr(VI) under this condition.

6. Study of Adsorption Thermodynamics

Fig. S2 shows that the adsorption capacity of CR and Cr(VI) increased with increasing temperature. The values of ΔH^0 and ΔS^0 were obtained from the intercept and slop of $\ln K_d$ versus 1/T following formula (8), (9) and (10) [43,44] (Fig. S3). The value of Gibbs free energy (ΔG^0), enthalpy (ΔH^0), and entropy (ΔS^0) are listed in Table 3. The two ΔH^0 values are positive, indicating that CR and Cr(VI) adsorption by GO/MS@HBP is endothermic. In addition, ΔG^0 is negative, indicating that the adsorption process is spontaneous, while positive value of ΔS^0 indicates that the disordered solid-liquid interface is enhanced.

$$\ln K_d = \frac{\Delta S^0}{R} - \frac{\Delta H^0}{RT} \quad (8)$$

$$\Delta G^0 = \Delta H^0 - T\Delta S^0 \quad (9)$$

$$K_d = \frac{q_e}{C_e} \quad (10)$$

where K_d is the adsorption equilibrium constant (L kg^{-1}); R is the gas molar constant (8.314 J mol^{-1}·K^{-1}); T is the relative temperature (K); ΔS^0 (kJ mol^{-1}), ΔH^0 (kJ mol^{-1}) and ΔG^0 (kJ mol^{-1}) are three thermodynamic parameters: entropy, enthalpy and Gibbs free energy.

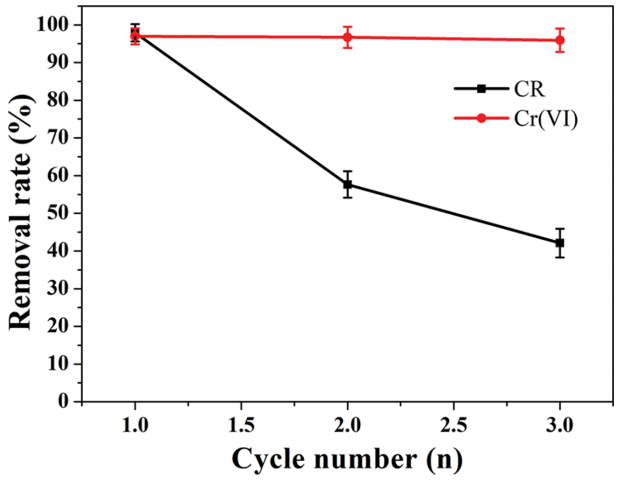

Fig. 13. Reusability of GO/MS@HBP.

7. Regeneration Performance Research Experiment

The removal rate by GO/MS@HBP after three cycles is shown in Fig. 13. The removal rate of Cr(VI) is more than 90% after three cycles, while CR removal rate decreased to 42%. GO/MS@HBP could be used repeatedly and maintain a high removal rate, especially for Cr(VI), indicating that GO/MS@HBP is an adsorbent with good practical application value.

CONCLUSIONS

Grafting method was used to synthesize GO/MS@HBP composite material, and the ability of GO/MS@HBP to remove Cr(VI) and CR by adsorption under different conditions was studied. The results showed that the optimal conditions for GO/MS@HBP to adsorb Cr(VI) and CR are 20 mg of adsorbent, 6 h adsorption time, and pH 2 and 10 mg of adsorbent, adsorption time of 8 h, and pH 5-9. The synthesized GO/MS@HBP adsorbent had a better removal rate for Cr(VI) (100%) and CR (99.46%). The Langmuir isotherm adsorption model showed that CR and Cr(VI) were adsorbed by GO/MS@HBP by monolayer adsorption. The adsorption thermodynamics study showed that the adsorption of CR and Cr(VI) by GO/MS@HBP was endothermic, and high temperature was conducive to adsorption. Competitive adsorption showed that GO/MS@HBP had a good selectivity for Cr(VI) and CR. Regeneration experiments showed that GO/MS@HBP removed 90% of Cr(VI) after three cycles. Therefore, the high adsorption capacity and removal rate indicated that the reusable material GO/MS@HBP could be used as an effective adsorbent for removing CR and Cr(VI).

SUPPORTING INFORMATION

Additional information as noted in the text. This information is available via the Internet at http://www.springer.com/chemistry/journal/11814.

REFERENCES

1. M. N. V. R. Kumar, T. R. Sridhari, K. D. Bhavani and P. K. Dutta, *Bior. Techn.*, **45**, 25 (1998).
2. K. G. Bhattacharyya and N. Sarma, *Indian J. Chem. Techn.*, **4**, 237 (1997).
3. M. N. Ahmed and R. N. Ram, *Environ. Pollut.*, **77**, 79 (1992).
4. S. P. Das, C. Shamik, M. Madhurim and S. Keka, *Sep. Sci. Tech-*

nol., **47**, 112 (2012).
5. A. Mittal, J. Mittal, A. Malviya and V. K. Gupta, *J. Colloid Interface Sci.*, **340**, 16 (2009).
6. A. K. Shanke, C. Cervantes, H. Loza-Tavera and S. Avudainayagam, *Environ. Int.*, **31**, 739 (2005).
7. S. Rumpa, N. Rumki and S. Bidyut, *J. Coord. Chem.*, **64**, 1782 (2011).
8. C. Carlos, C. G. Jesús, D. Silvia, G. C. Félix, L. C. Herminia, T. G. Juan Carlos and M. S. Rafael, *FEMS. Microbiol. Rev.*, **25**, 335 (2001).
9. R. J. Bruce, *Environ. Sci. Techn.*, **30**, 248A (1996).
10. H. Lachheb, E. Puzenat, A. Houas, M. Ksibi, E. Elaloui, C. Guillard and J. M. Herrmann, *Appl. Catal. B-Environ.*, **39**, 75 (2002).
11. E. Lorenc-Grabowska and G. Gryglewicz, *Pigments*, **74**, 34 (2007).
12. Y. B. Zhou, J. Lu, Y. Zhou and Y. D. Liu, *Environ. Pollut.*, **252**, Pt A (2019).
13. N. Kongsricharoerm and C. Polprasert, *Water Sci. Technol.*, **34**, 109 (1996).
14. S. Rengaraj, K. H. Yeon and S. H. Moon, *J. Hazard. Mater.*, **87**, 273 (2015).
15. R. Saha, R. Nandi and B. Saha, *J. Coord. Chem.*, **64**, 1782 (2011).
16. Y. Tadjenant, N. Dokhan, A. Barras, A. Addad and R. Boukherroub, *Chemosphere*, **258**, 127316 (2020).
17. N. S. Bolan, *J. Environ. Qual.*, **37**, 1299 (2008).
18. K. Kadirvelu, M. Kavipriya, C. Karthika, M. Radhika, N. Vennilamani and S. Pattabhi, *Bior. Techn.*, **87**, 129 (2003).
19. L. Ren, H. Lin, F. Meng and F. Zhang, *Ceram. Int.*, **7**, 45 (2018).
20. A. ZabihiSahebi, S. Koushkbaghi, M. Pishnamazi, A. Askari, R. Khosravi and M. Irani, *Int. J. Biol. Macromol.*, **140**, 1 (2019).
21. M. R. Abukhadra, A. Adlii and B. M. Bakry, *Int. J. Biol. Macromol.*, **126**, 1 (2019).
22. L. Anton, H. Heyong, F. Michael and K. Jacek, *J. Phys. Chem. B*, **102**, 4477 (1998).
23. M. Hirata, T. Gotou and M. Ohba, *Carbon*, **43**, 503 (2005).
24. E. Mahmoudi, S. Azizkhani, A. W. Mohammad and L. Y. Ng, *J. Environ. Sci.*, **98**, 151 (2020).
25. Q. Liu, J. B. Shi, J. Sun and G. Jiang, *Angew. Chem. Int. Ed.*, **50**, 5913 (2011).
26. L. Li, Z. Guojun, Y. Benqun, L. Xu and X. Shan, *ACS Appl. Nano. Mater.*, **9**, 4695 (2018).
27. X. H. Li, *Chem. Eng. J.*, **273**, 630 (2015).
28. B. Wca, B. Jwa, B. Zl, L. B. Yan, C. Jz and B. Bh, *Colloid Surf. A.*, **563**, 102 (2019).
29. Y. Tan, Z. Sun, H. Meng, Y. Y. Han and X. Zhang, *Powder Technol.*, **356**, 162 (2019).
30. F. Song, Y. Li, S. Wang, L. Zhang and Q. Chen, *New. J. Chem.*, **43**, 17284 (2019).
31. Y. S. Ho and G. McKay, *Process Biochem.*, **34**, 451 (1999).
32. A. Silva, K. S. Sousa, A. S. Germano, V. Oliveira, J. P. Espínola, G. Maria, M. Fonsec, C. Airoldi, T. Arakaki and L. N. H. Arakaki, *Colloid Surf. A.*, **332**, 144 (2009).
33. A. Boonpoke, S. Chiarakorn, N. Laosiripojana and A. Chidthaisong, *Environ. Prog. Sustain.*, **35**, 1716 (2016).
34. V. A. Chhabra, A. Deep, R. Kaur and R. Kumar, *Int. J. Sci. Emerging Technologies with Latest Trends.*, **4**, 13 (2012).
35. X. Sun, L. Yang, H. Xing, J. Zhao, X. Li and H. Liu, *Chem. Eng. J.*, **234**, 338 (2013).
36. L. Zhang, F. Song, S. Wang, H. Wang, W. Yang and Y. Li, *J. Chem. Eng. Data*, **65**, 9 (2020).
37. J. H. Zhu, S. Y. Wei, H. B. Gu, S. B. Rapole, Q. Wang, Z. P. Luo, N. Haldolaarachchige, D. P. Young and Z. H. Guo, *Environ. Sci. Technol.*, **46**, 2 (2012).
38. P. Ding, K. L. Huang, G. Y. Li and W. W. Zeng, *J. Hazard. Mater.*, **146**, 58 (2007).
39. D. L. Zhao, X. Gao, C. Wu, R. Xie, S. Feng and C. L. Chen, *Appl. Surf. Sci.*, **384** (2016).
40. R. Zhao, X. Li, B. L. Sun, Y. Z. Li, Y. Li, R. Yang and C. Wang, *J. Mater. Chem. A*, **5**, 3 (2017).
41. H. L. Vasconcelos, T. P. Camargo, N. S. Gonçalves, A. Neves, M. C. M. Laranjeira and V. T. Fávere, *Funct. Polym.*, **68**, 572 (2008).
42. C. Gervas, E. B. Mubofu, J. E. G. Mdoe and N. Revaprasadu, *J. Porous. Mat.*, **23**, 1 (2015).
43. J. P. Maity, C. M. Hsu, T. J. Lin, W. C. Lee, P. Bhattacharya, J. Bundschuh and C. Y. Chen, *Environ. Nanotechnol., Monit. Manag.*, **9**, 18 (2018).
44. A. Heidari, H. Younesi and Z. Mehraban, *Chem. Eng. J.*, **153**, 70 (2009).

Supporting Information

Simultaneous removal of Congo red and Cr(VI) using amino-modified GO/MS composite materials

Liang Cheng*,†, Li Zhang, Hongxia Wang**, and Fangxiang Song****

*School of Electrical Engineering, Guizhou University, Guiyang 550025, China
**College of Chemistry and Chemical Engineering, Guizhou University, Guiyang 550025, China
(*Received 3 August 2021 • Revised 31 October 2021 • Accepted 29 November 2021*)

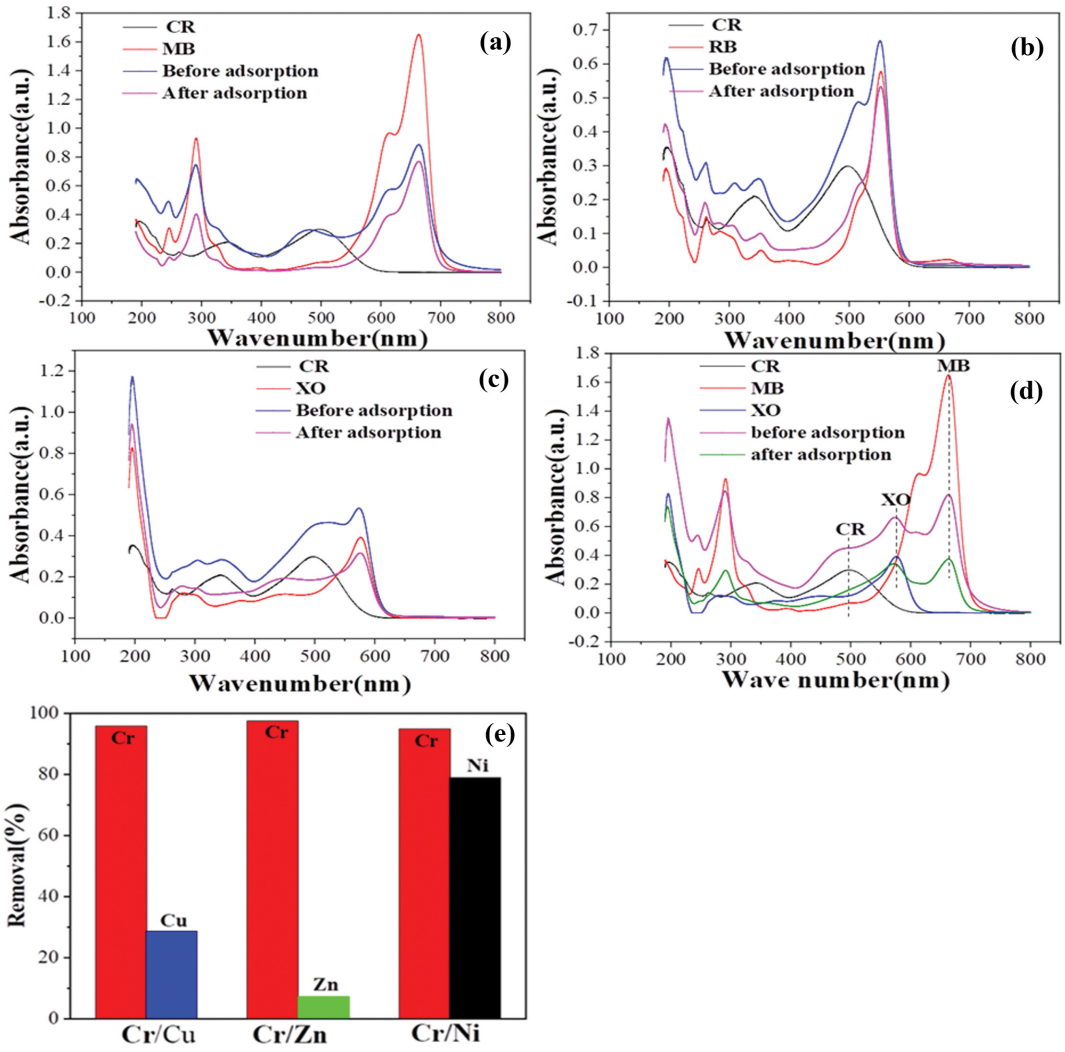

Fig. S1. Adsorption spectra of CR and other dye contaminants in a mixed solution ((a), (b), (c), (d)); removal of Cr(VI) and different heavy-metal ions in a mixed solution (e).

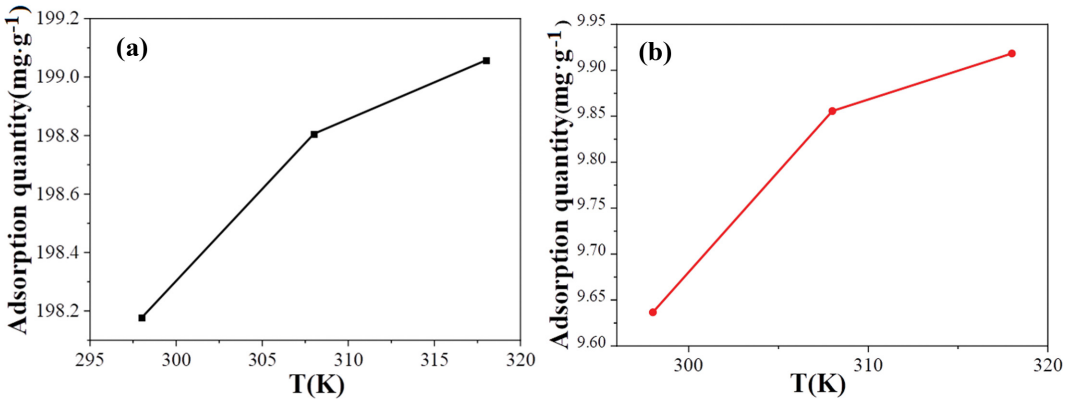

Fig. S2. Effect of the different temperatures of GO/MS@HBP on CR (a) and Cr(VI) (b) adsorption.

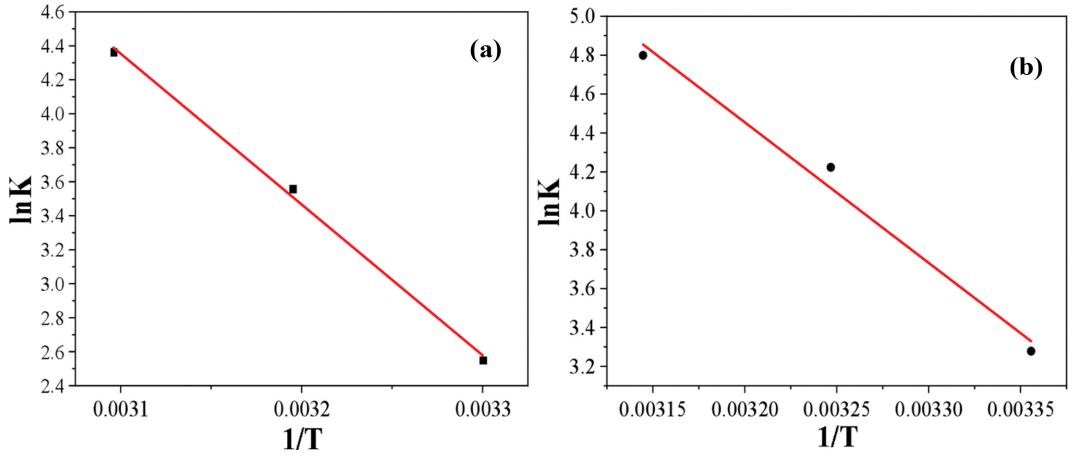

Fig. S3. Fitted curves of CR (a) and Cr(VI) (b) adsorption on GO/MS@HBP.

Table S1. Pore Texture Parameters of GO/MS@CN and GO/MS@HBP

Materials	S_{BET} ($m^2 \cdot g^{-1}$)	Va ($cm^3 \cdot g^{-1}$)	Da (nm)
GO/MS	125.67	0.21	2-4
GO/MS@CN	81.26	0.16	2-4
GO/MS@HBP	49.32	0.11	2-5.5

Where S_{BET} is the BET specific surface area, Va is the BJH adsorption cumulative volume of pores, and Da is the BJH adsorption average pore diameter.

Table S2. Comparison of Cr(VI) adsorption performance of GO/MS@HBP and other materials

Adsorbent	Adsorption conditions				Q_e (mg/g)	Ref.
	C_0 (mg/L)	Dosage (mg)	Adsorption time	pH		
n-GO@HTCS[a]	100	100	50 min	---	42.64	[1]
PVDF-HFP[b]	100	10	24 h	4.5	15.08	[2]
Fe-MCNS[c]	50	20	---	3	87	[3]
AMS-MNPs[d]	20	35	30 min	2	13.905	[4]
Co-condensation GO/MS@HBP	10	20	1 h	2	92.251	[5]
Postgrafting GO/MS@HBP	10	20	6 h	2	93.7286	In this work

[a]n-GO@HTCS: nano-graphene oxide assisted hydrotalcite/chitosan biocomposite
[b]APVDF-HFP: polyaniline-coated polyvinylidenefluoride-co-hexafluoropropilene
[c]Fe-MCNS: iron-containing magnetic mesoporous carbon nanospheres
[d]AMS-MNPs: APTES-grafted mesoporous silica magnetite nanoparticles

REFERENCES

1. S. Periyasamy, P. Manivasakan, C. Jeyaprabha, S. Meenakshi and N. Viswanathan, *Int. J. Biol. Macromol.*, **132**, 1068 (2019).
2. G. Dognani, P. Hadi, H. Ma, F. C. Cabrera, A. E. Job, D. L. Agostini and B. S. Hsiao, *Chem. Eng. J.*, **372**, 341 (2019).
3. S. Li, L. Liu, Y. Yu, G. Wang, H. Zhang and A. Chen, *J. Alloy. Compd.*, **698**, 20 (2017).
4. S. H. Araghi, M. H. Entezari and M. Chamsaz, *Micropor. Mesopor. Mater.*, **218**, 101 (2015).
5. L. Zhang, F. Song, S. Wang, H. Wang, W. Yang and Y. Li, *J. Chem. Eng. Data*, **65**, 9 (2020).